International Journal of Hydrogen Energy 166 (2025) 151006

Contents lists available at ScienceDirect

International Journal of Hydrogen Energy

journal homepage: www.elsevier.com/locate/he

Towards decarbonizing gas: A generic optimal gas flow model with linepack constraints for assessing the feasibility of hydrogen blending in existing gas networks

Gabriele Guzzo [a,*], Sleiman Mhanna [b], Isam Saedi [b,c], Carlo Carcasci [a], Pierluigi Mancarella [b,d]

[a] DIEF: Department of Industrial Engineering, University of Florence, via Santa Marta, 3, 50139, Florence, Italy
[b] Department of Electrical and Electronic Engineering, University of Melbourne, Parkville, Melbourne, VIC, 3052, Australia
[c] Department of Electromechanical Engineering, University of Technology, Al-Wehda neighborhood, Baghdad, Iraq
[d] Department of Electrical and Electronic Engineering, University of Manchester, Oxford Rd., Manchester, M13 9PL, United Kingdom

ARTICLE INFO

Handling editor: B Shabani

Keywords:
Hydrogen
Pipeline optimization
Gas network modelling
Hydrogen blending
Linepack
Transient model

ABSTRACT

Hydrogen blending into natural gas networks is a promising pathway to decarbonize the gas sector but requires bespoke fluid-dynamic models to accurately capture the properties of hydrogen and assess its feasibility. This paper introduces a generalizable optimal transient gas flow model for transporting homogeneous natural gas-hydrogen mixtures in large-scale networks. Designed for preliminary planning, the model assesses whether a network can operate under a given hydrogen blending ratio without violating existing constraints such as pressure limits, pipeline and compressor capacity. A distinguishing feature of the model is a multi-day linepack management strategy that engenders realistic linepack profiles by precluding mathematically feasible but operationally unrealistic solutions, thereby accurately reflecting the flexibility of the gas system. The model is demonstrated on Western Australia's 7560 km transmission network, using real system topology and demand data from several representative days in 2022. Findings reveal that the system can accommodate up to 20 % mol hydrogen, potentially decarbonizing 7.80 % of gas demand.

Nomenclature

Latin Symbols		
A:	Pipe cross-sectional area	[m^2]
A^z:	SRK coefficient	[−]
B^z:	SRK coefficient	[−]
c:	Specific cost	[$/MJ]
C:	Capacity	[TJ/d]
D:	Pipe diameter	[m]
f:	Friction factor	[−]
HHV:	Higher heating value	[MJ/Sm^3]
J:	Number of discretized segments	[−]
L:	Pipe length	[m]
LHV:	Lower Heating Value	[MJ/Sm^3]
Lp:	Linepack	[MJ]
M:	Molar mass	[kg/kmol]
N:	Number of days	[−]
$\dot{m}$:	Mass flow rate	[kg/s]
T:	Temperature	[K]
p:	Discretized nodes pressure	[Pa]
P:	Real nodes pressure	[Pa]
r:	Pressure ratio	[−]
R:	Gas constant	[J/(mol•K)]
SG:	Specific Gravity	[−]
t:	Time	[s]
V:	Vector of variables	[−]
W:	Power	[MW]
y:	Molar fraction	[−]
Z:	Compressibility factor	[−]

Greek Symbols

ρ:	Density	[kg/m^3]
γ:	Isentropic exponent	[−]

(continued on next page)

* Corresponding author.
E-mail addresses: gabriele.guzzo@unifi.it (G. Guzzo), sleiman.mhanna@unimelb.edu.au (S. Mhanna), isaedi@student.unimelb.edu.au (I. Saedi), carlo.carcasci@unifi.it (C. Carcasci), pierluigi.mancarella@unimelb.edu.au (P. Mancarella).

https://doi.org/10.1016/j.ijhydene.2025.151006
Received 13 April 2025; Received in revised form 11 August 2025; Accepted 13 August 2025
Available online 18 August 2025

(*continued*)

η:	Efficiency	[−]
ω:	Linepack term	[−]
ε:	Roughness	[m]

Sets

$\mathscr{C}$:	Compressors
$\mathscr{G}$:	Days
$\mathscr{N}$:	Nodes
$\mathscr{P}$:	Pipes
$\mathscr{S}$:	Suppliers
$\mathscr{T}$:	Timesteps
$\mathscr{X}$:	Discretized nodes

Subscripts and Superscripts

ave:	Average
c	compressor (W_c, η_c)
D	Demand
f	Fuel
g	Gas
i,j	Node indexes
ij	Pipe-compressor indexes
loss	Losses
mass	Unit of mass (HHV_{mass}, LHV_{mass})
pm	Prime mover
s	Supply
std	Standard
th	Gas energy flow rate
u	Universal
y_{H2}	H_2 molar fraction
x	Discretized nodes index

Acronymous

AEMO	Australian Energy Market Operator
CS	Compressor station
DBNGP	Dampier to Bunbury natural gas pipeline
GFG	Gas-fired generators
GGP	Goldfields gas pipeline
NG	Natural gas
NPK	Nikuradse-Prandtl-von Karman
OGF	Optimal gas flow
PDEs	Partial differential equations
SRK	Soave-Redlich-Kwong
TGP	Telfer gas pipeline
WA	Western Australia

Constants

T_{std}:	288.15	[K]
p_{std}	101325	[Pa]
R_u	8314.5	[J/(mol•K)]
R_{air}	286.71	[J/(kg•K)]
γ	1.35	[−]
η_c	0.8	[−]
η_{pm}	0.3	[−]

1. Introduction

Natural gas (NG) plays a significant role in global energy systems. Primarily utilized for heating, industrial processes, electricity generation, and as a fuel for vehicles, its applications are widespread and vary by country [1]. Its popularity stems from being a relatively cleaner fossil fuel compared to coal and oil. However, as concerns about climate change and greenhouse gas emissions have grown, the role of NG in the energy transition has become a subject of debate [2,3]. One of the options considered to phase out NG concerns the establishment of a hydrogen (H_2) economy, which could represent a green alternative capable of retaining some of its advantages, such as the ability to be stored and transported over long distances in gaseous or liquid form [4], making it a preferable investment choice than power cables for high RES capacities transmitted over medium to long distances [5,6].

Blending H_2 into the current network infrastructure is a potential strategy to boost the development of the H_2 economy and reduce dependence on NG. Numerous projects worldwide are supporting this initiative [7,8]. Nonetheless, the distinct thermochemical properties of NG and H_2 pose challenges concerning gas quality at end-users [9], material compatibility due to hydrogen embrittlement [10], increased leakage risk [11], and the fluid-dynamic variations affecting the operations of pipelines, compressors, and regulating stations [12,13]. Localized H_2 injections may result in complex evolutions of the gas composition in the downstream flow [14–18], necessitating significant investments in sensors and meters to control gas quality in topologically complex networks. In this scenario, hardware investments must be coupled with computationally intensive fluid dynamic models able to track H_2 [19] and control strategies to maximize the H_2 injection and, at the same time, comply with quality limits at the end-users [20,21]. Recent studies have proposed advanced modeling approaches to address these challenges. Clees et al. [22] presented a high-fidelity simulation framework for hydrogen injection in long-distance pipelines, using non-isothermal transient models and GERG-2008 to capture gas property variations. Zhou et al. [23] investigated an electricity-gas-hydrogen coupled system for Ireland, demonstrating how hydrogen blending can support the integration of renewables and reduce emissions. Similarly, Qiu et al. [24] developed an integrated optimization model for electricity-gas systems, highlighting the impact of hydrogen on gas dynamics and proposing advanced control strategies for safe and efficient operation. Given the complexity of controlling and coordinating the injections, if technically feasible, operators could benefit from uniformly pre-mixing H_2 and NG at network entry points, such as gas fields, import points, entry stations, or pipelines, to ensure a consistent composition downstream. However, maintaining a constant H_2 mole fraction in the downstream gas flow can address the quality control problem, but it does not ensure compliance with the network's fluid-dynamic constraints, such as offtake pressure and compressor capacity [25].

Hence, to assess the feasibility of transporting homogeneous NG-H_2 blends, it is essential to develop gas network models that can accurately capture the fluid dynamics. These models can be essential to help decision-makers make informed choices about the green transition of gas networks. In light of this need, several works presented steady-state models to investigate the fluid-dynamic consequences of transporting NG-H_2 blends [25–29]. These studies highlighted several fluid-dynamic issues such as larger gas flow rates and velocities to meet the same energy demand [25,26,28,29], reduced pipeline capacity [26,28,29], higher pressure losses [25,27–29], and power consumption at compressor stations [29].

However, steady-state models cannot capture the inherent dynamics of pipelines caused by variable demand (slow transients) or the closing of valves and compressors shut off (fast transients). Therefore, to capture dynamic phenomena, authors proposed transient gas flow models for homogeneous NG-H_2 blends [30–33].

The models presented in Refs. [30–33] were tested considering several NG-H_2 homogeneous mixtures on fictitious pipeline systems [31,32] or real but topologically simple pipeline sections such as a part of the Yamal-Europe gas pipeline [30] and the Greenstream pipeline [33]. Cavana et al. [33] showed that for H_2 molar contents higher than 5 % mol, pressure at the offtake point of the Greenstream pipeline fell below the required technical minimum. Furthermore, Uilhoorn [30] affirmed that the pressure drop increase, in conjunction with the H_2-induced linepack decrease, may present difficulties in the short-term balancing of supply and demand. Elaoud et al. [32] analyzed a transient scenario caused by the sudden closure of delivery nodes with a linear closure law. The findings indicate that transient pressure waves generated by the valve closure in H_2 and NG-H_2 mixtures reach higher pressure values than those of NG, posing risks in overcoming the maximum allowable operating pressure of the pipeline [32]. Guzzo et al. [34] presented a quantitative analysis of the relationships between variations in key gas properties, including compressibility factor, higher heating value and specific gravity, and changes in pressure loss, linepack, and compressor consumption. The results show that increasing hydrogen blending leads to sublinear increases in the compressibility factor, linear decreases in volumetric higher heating value and specific gravity, and, consequently, a nonlinear and non-monotonic increase in pressure losses, greater compressor power consumption, and a reduction in linepack capacity. Furthermore, in the analysis, the authors highlighted that H_2 presents a faster dynamic response to demand variation compared to NG. The results showed also that H_2 induces larger pressure swings, thereby underscoring the potential risks associated with pipeline fatigue failure.

The literature presented so far represents state-of-the-art fluid-dynamic models capable of accurately simulating homogeneous blends of NG and H_2. A common finding across these studies is that transporting NG-H_2 blends often leads to fluid-dynamic challenges such as offtake pressure exceeding constraint limits under given boundary conditions. However, due to their intrinsic nature, simulation models can simulate problems under specific boundary conditions but are not suitable for comprehensive feasibility studies on large-scale systems. Conducting such studies with simulation models requires computationally intensive parametric analyses to investigate the feasibility of operating the system within the space of acceptable solutions defined by existing constraints. Hence, to conduct comprehensive H_2 blending feasibility studies on complex systems, such as real gas transmission networks, fluid-dynamic models must be embedded in optimization frameworks.

This work presents a generic model to conduct fluid-dynamic feasibility studies on H_2 blending in real networks considering a multi-day gas network operation scheduling horizon. Gas network operation scheduling problems involve coordinating the activities of compressors, suppliers and pipelines to ensure the efficient, safe, and reliable transport of gas. From the perspective of pipeline operators, operation scheduling tasks translate into optimization problems aimed at minimizing fuel costs or maximizing throughput in pipeline transmission networks, as well as addressing short-term storage issues like linepacking management [35–37], subject to gas network operational constraints. Fuel cost minimization problems typically involve the minimization of compressor power [38,39] or fuel consumption [37,40,41]. Instead, market operators have the primary objective to ensure equitable and transparent access to the gas transportation network. They are therefore recognized as neutral entities who undertake the operation problem of allocating pipeline capacity to pipeline operators to minimize resource consumption while also upholding system safety [42].

In literature, the neutral operator perspective is adopted in the context of optimal gas flow (OGF) models embedded in the coordinated operation of NG and electricity systems problems, where the perspective of the neutral operator aligns with that of regulatory entities responsible for impartially coordinating and regulating network operators [16,18,43–45]. The complexity of modelling OGF problems lies in the strong nonlinearity of the constraints. Most authors simplify the optimization problem through steady-state gas flow models [18,36,37,40,41,46] but only transient or quasi-dynamic models [38,39,44,45,47–49] can capture the dynamic of the network. Modelling the pipeline dynamics is essential to capture linepack, which plays a crucial role in balancing intraday supply and demand mismatches in real systems [49]. However, implementing transient models without constraining linepack in OGF problems can lead to misleading results. In fact, linepack can be interpreted by the model as a zero-cost source of NG and therefore preferred over supply sources to minimize the gas supplied. Relying on linepack to meet demand instead of directly supplying gas results in a reduction in network pressure, thereby diminishing the system's capacity to handle unforeseen events. Nevertheless, only a limited number of works considered linepack constraints in the operation scheduling problem [16,47–49]. Posada et al. [47] included among the constraints a linepack target for the end of the day, while Ameli et al. [48] imposed a penalty cost to linepack usage in the optimization function. Furthermore, it is noteworthy that a limited number of the previously mentioned OGF models can handle NG-H_2 mixtures, either for homogeneous flows [36,50] or in tracking algorithms [16,18]. Among these, only Mhanna et al. [16] implemented a transient gas flow model, but the authors only evaluated linepack without incorporating any target into the optimization function. This is evidenced by the linepack reduction observed in their results at the end of the optimization horizon.

In light of this background, there is a need for a modelling framework capable of properly assessing the feasibility of transporting NG-H_2 blends in large scale networks considering linepack constraints. To address this gap, this work presents an optimization framework for gas transmission networks that incorporates an isothermal transient gas flow model for horizontal pipelines transporting NG-H_2 homogeneous blends. The model explicitly accounts for the physical properties of the mixture, compressibility factor, density, and higher heating value, which are modelled as functions of the hydrogen concentration. This ensures that the fluid-dynamic effects associated with hydrogen blending are consistently represented within the optimization formulation. The proposed isothermal formulation and horizontal pipeline assumption are well suited for networks with characteristics such as buried pipelines in flat terrain and high operating pressures. In other contexts, such as networks operating at lower pressures with significant elevation changes, large seasonal or spatial temperature variations, or multiple hydrogen injection points, non-isothermal formulations, inclined-pipe models, or compositional tracking algorithms may be required. The generic optimization framework presented here can accommodate such extensions, although these would entail greater model complexity and additional data requirements. Moreover, although the optimization is conducted from the perspective of a neutral operator, the model is general and can be adapted to different stakeholders' perspectives by modifying the optimization function. To capture realistic network operation, the model includes a gas supply strategy aimed at minimizing the use of resources ensuring the continuous system capacity to cope with unforeseen events by also minimizing the linepack difference between the beginning and end of each day.

From a modelling perspective to the best of the authors' knowledge, this is the first work.

- presenting an optimization framework embedding a transient gas flow model for homogeneous NG-H_2 mixtures that also considers linepack constraints in the scheduling problem. A replicable case study is used to compare the results of the OGF proposed to those of a standard OGF that minimizes only the gas supplied. The aim is to demonstrate that incorporating linepack management strategies in the OGF model is crucial for mirroring realistic network operations. This ensures a consistent level of flexibility at the end of the gas day, avoiding solutions with unrealistic progressive linepack reductions obtained with standard OGF models.
- Presenting a transient OGF model developed to study the feasibility of transporting homogeneous NG-H_2 blends in large-scale gas transmission networks considering a multi-day scheduling horizon. The robustness of the model is demonstrated on Western Australia's (WA) gas transmission network that, to the best of the authors' knowledge, represents the largest gas network analyzed with a transient model in the literature.

The remainder of the paper is structured as follows. Section 2 presents the modelling methodology, introducing a transient OGF formulation for homogeneous NG-H_2 mixtures and detailing the inclusion of linepack constraints in the optimization problem. Section 3 introduces two case studies: a benchmark single-pipeline system used to validate the model's dynamic behavior and to assess the role of linepack management, and the WA gas transmission network, employed to test the model's scalability and realism. Section 4 presents the simulation results, demonstrating how linepack constraints influence supply strategies and evaluating the fluid-dynamic feasibility of different H_2 blending

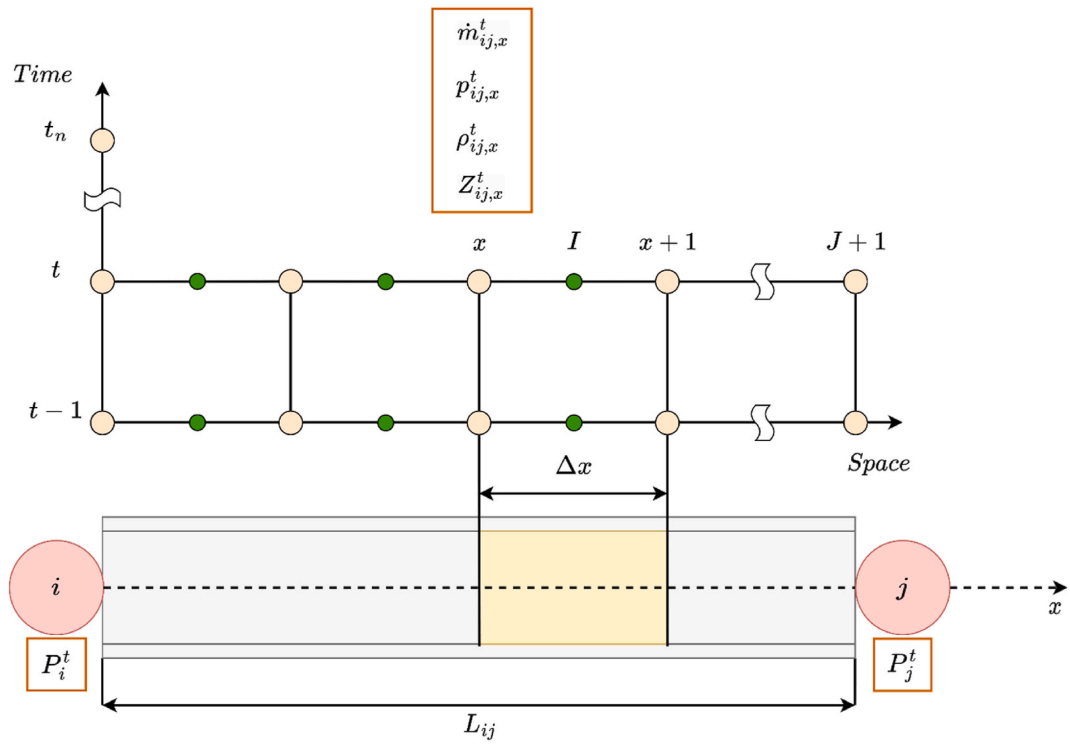

Fig. 1. Pipeline discretization scheme.

levels in the WA network. The paper concludes in Section 5 by summarizing the findings and outlining the implications for gas network operators and hydrogen integration policies.

2. Optimal gas flow model

2.1. Transient gas network model

A gas network is a graph where elements such as nodes, pipes, and compressors are connected. To describe the model equations, the following sets are introduced: $\mathscr{P}$ the set of pipes, $\mathscr{N}$ the set of nodes, C the set of compressors, $\mathscr{S}\subset\mathscr{N}$ the set of supply, $\mathscr{T}$ the set of time steps defining the time horizon. The transient gas flow model introduced in this paper for optimization purposes is based on the model presented by Guzzo et al. [34], which was originally developed for simulation studies and rigorously validated against the state-of-the-art commercial gas network software PipelineStudio® by Emerson. This validation, detailed in Guzzo et al. [34], covered hydrogen blending scenarios from 0 % to 100 % mol and demonstrated strong agreement in pressure profiles, with average errors below 0.75 %, confirming the robustness and accuracy of the fluid-dynamic formulation used here.

The model presented in this study adopts a horizontal pipe configuration, with the axial position denoted by the variable " x" under the hypothesis of one-dimensional isothermal flow and creeping motion [51]. The isothermal assumption is justified by the relatively slow gas velocities and the thermal inertia of buried pipelines, which allow the gas to equilibrate with the surrounding soil temperature. This modeling approach, also adopted and validated in Ref. [51], enables a tractable yet accurate representation of gas flow dynamics for system-level analyses when detailed spatial data on ground thermal properties and boundary heat transfer conditions are not available.

The partial derivative equations (PDEs) that describe the gas flow in a pipeline are represented by Equations (1) and (2).

$$\frac{\partial \rho}{\partial t}+\frac{1}{A}\frac{\partial \dot{m}}{\partial x}=0 \tag{1}$$

$$\frac{\partial p}{\partial x}+\frac{1}{A}\frac{\partial \dot{m}}{\partial t}+\frac{8f\dot{m}|\dot{m}|}{\rho\pi^2D^5}=0 \tag{2}$$

To solve the PDEs, a fully implicit discretization scheme centered in space and forward in time given its intrinsic stability is adopted. Fig. 1 shows the discretization scheme for a pipeline $ij\in\mathscr{P}$ that connects two nodes $i,j\in\mathscr{N}$. Each pipeline is discretized in $J_{ij}=\left\lceil\frac{L_{ij}}{\Delta x_{ij}}\right\rceil$ segments corresponding to a set $\mathscr{X}$ containing $(J_{ij}+1)$ nodes. The variables stored in the nodes created by the discretization scheme are $(\dot{m}^t_{ij,x}\ ,\ p^t_{ij,x}\ ,\ \rho^t_{ij,x}\ ,\ Z^t_{ij,x})_{ij\in\mathscr{P},x\in\mathscr{X}}$ which represents respectively the mass flow rate, the pressure, the density and the compressibility factor of the gas. Equations (3) and (4) present the relationship between nodal pressure, indicated by the variable P^t, and the pressure at the boundaries of the pipes.

$$P^t_i=p^t_{ij,x=0} \tag{3}$$

$$P^t_j=p^t_{ij,x=J_{ij}+1} \tag{4}$$

The discretized PDEs representing the continuity (Eq. (1)) and momentum (Eq. (2)) equations for a pipeline ij are presented in Equations (5) and (6).

$$\left(\frac{\rho^t_{ij,x+1}+\rho^t_{ij,x}}{2}-\frac{\rho^{t-1}_{ij,x+1}+\rho^{t-1}_{ij,x}}{2}\right)\frac{1}{\Delta t}+\left(\dot{m}^t_{ij,x+1}-\dot{m}^t_{ij,x}\right)\frac{1}{A_{ij}\cdot\Delta x_{ij}}=0\quad\forall\, ij\in\mathscr{P},x\in\mathscr{X},t\in\mathscr{T} \tag{5}$$

$$\frac{p^t_{ij,x+1}-p^t_{ij,x}}{2\Delta x_{ij}}+\frac{\dot{m}^t_{ij,x+1}-\dot{m}^{t-1}_{ij,x+1}+\dot{m}^t_{ij,x}-\dot{m}^{t-1}_{ij,x}}{4A_{ij}\Delta t}+\frac{2f_{ij}\left(\dot{m}^t_{ij,x}+\dot{m}^t_{ij,x+1}\right)\left|\dot{m}^t_{ij,x}+\dot{m}^t_{ij,x+1}\right|}{\left(\rho^t_{ij,x+1}+\rho^t_{ij,x}\right)\pi^2D^5_{ij}}=0\;\forall\, ij\in\mathscr{P},x\in\mathscr{X},t\in\mathscr{T} \tag{6}$$

Under the assumption of a steady-state condition, the continuity equation simplifies to a trivial identity, while the momentum equation simplifies in the generalized flow equation (Equation (7)).

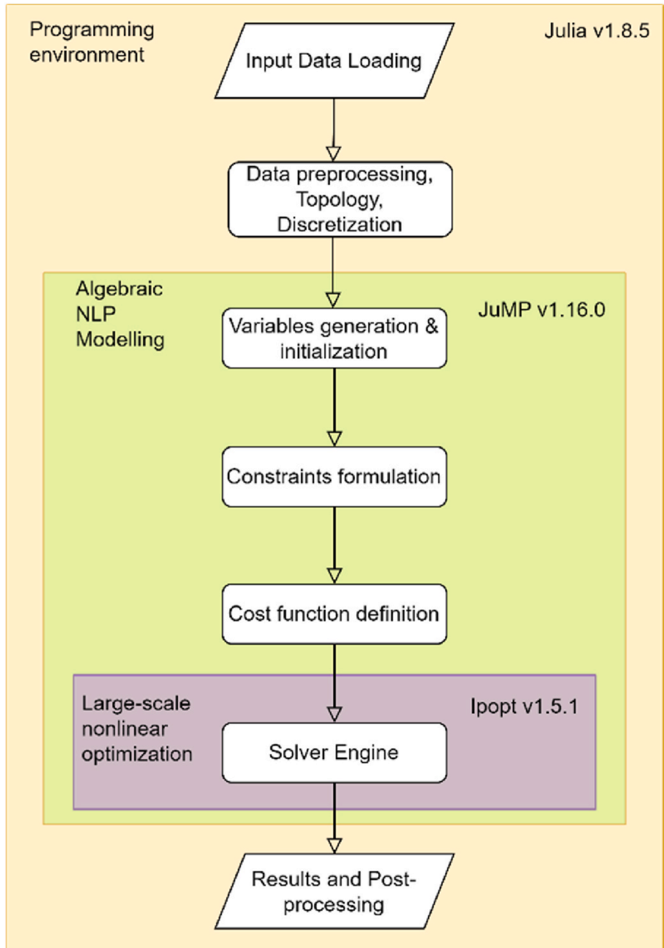

Fig. 2. Overview of the computational workflow.

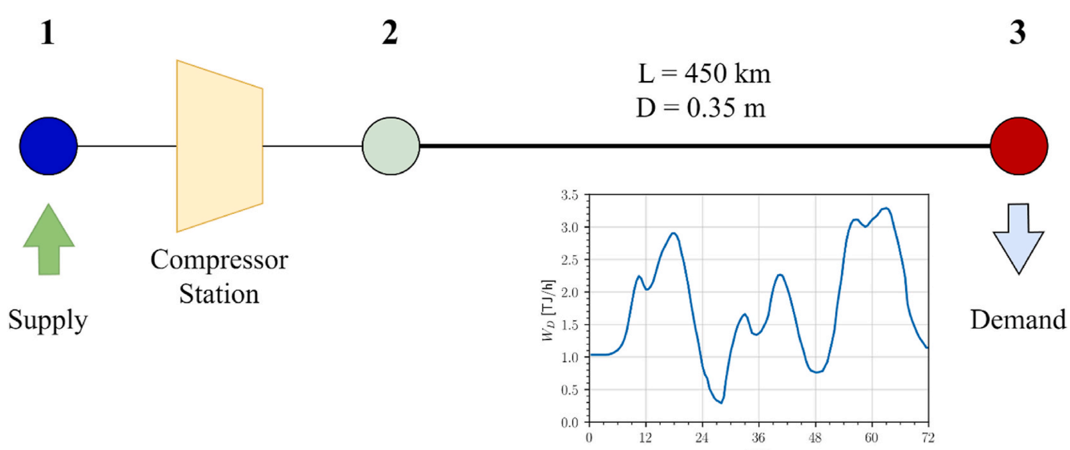

Fig. 3. Case study A: test system layout and demand profile.

Table 1
Case study A:gas network constraints.

	$\underline{p}$ [MPa]	$\bar{p}$ [MPa]	C [TJ/d]	r [–]	W [MW]
Node 1	5.0	5.0	100	–	–
Node 2	5.0	10.2	–	–	–
Node 3	3.5	10.2	–	–	–
Pipeline	–	–	100	–	–
Compressor	–	–	100	2.5	3.0

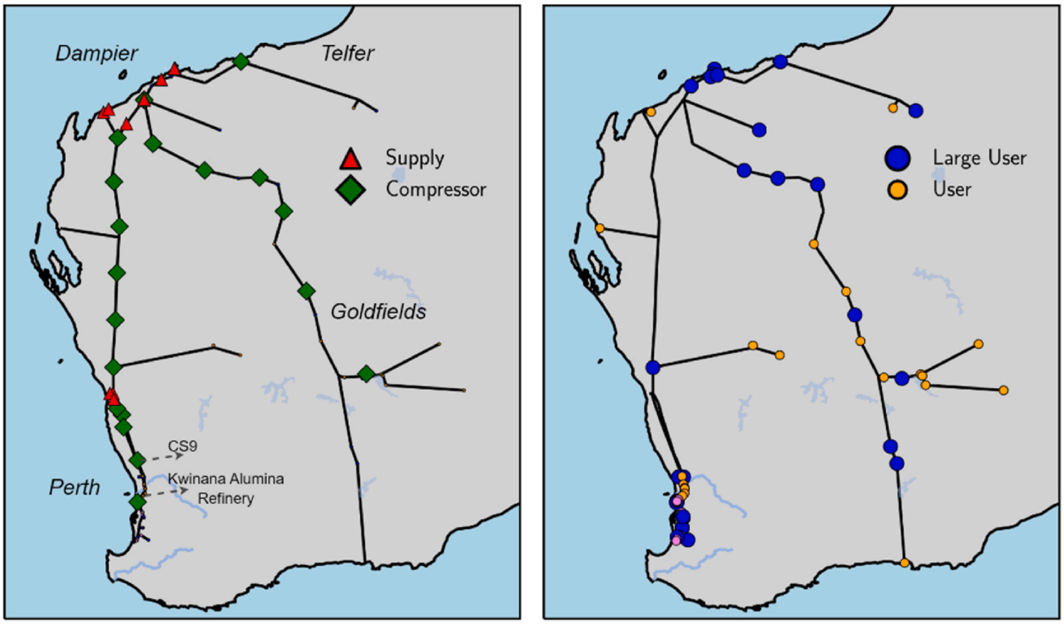

Fig. 4. Case study B: topology, supply, compressors and users of the WA gas system.

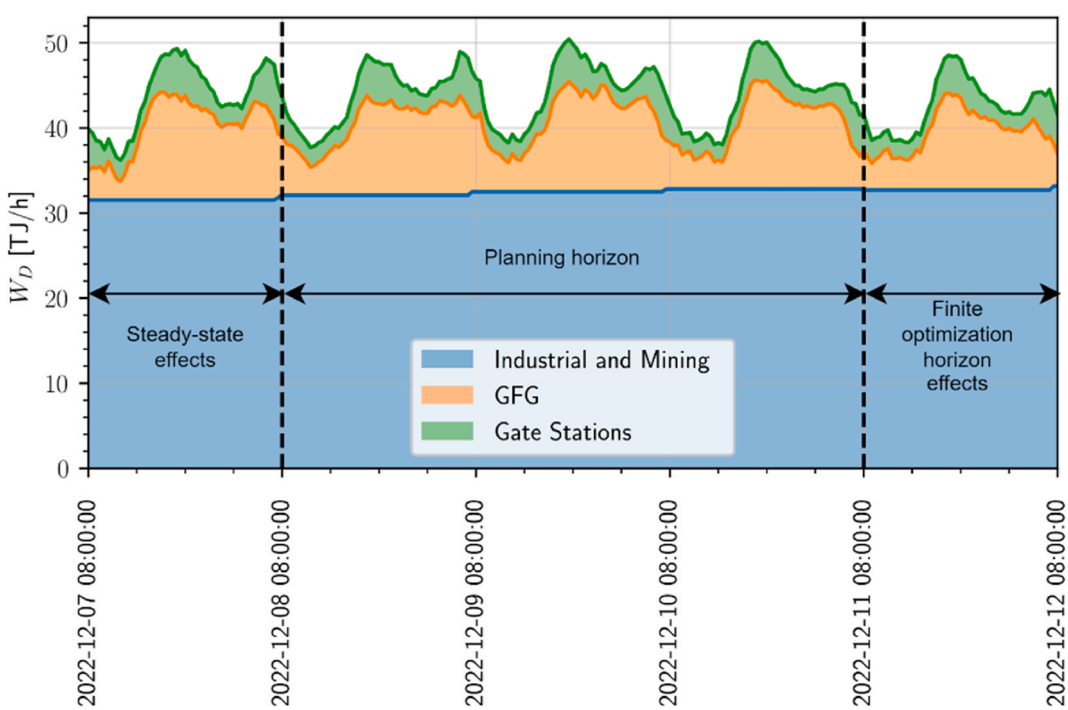

Fig. 5. Case study B: WA demand breakdown by sector for 5 representative days.

Table 2
Statistical descriptors of WA demand: 5 days considered vs 2022.

Descriptor	5 days values [TJ/h]	2022 values [TJ/h]
Mean	43.70	44.58
Std	3.62	3.50
Min	36.20	35.25
25 %	40.11	41.93
50 %	44.33	44.86
75 %	46.68	47.29
max	50.45	51.97

$$P_i^2 - P_j^2 = \frac{16}{\pi^2 R_{air}} \cdot \frac{f_{ij} SGL_{ij} Z_{ij} T}{D_{ij}^5} \left(\frac{p_{std}}{T_{std}}\right)^2 \cdot \left(\frac{\dot{m}_{ij}}{\rho_{std}}\right)^2 \forall\, ij \in \mathscr{P}, t = 0 \tag{7}$$

Equation (8) delineates the mass balance applied at each node and at each time step within the optimization horizon.

$$\sum_{s \in S_i} \dot{m}_s^t + \left(\sum_{ji \in P_{ji}} \dot{m}_{ji,x=J_{ij}+1}^t - \sum_{ij \in P_{ij}} \dot{m}_{ij,x=0}^t \right) + \left(\sum_{ji \in C_{ji}} \dot{m}_{ji}^t - \sum_{ij \in C_{ij}} \left(\dot{m}_{ij}^t + \dot{m}_{f_{ij}}^t \right) \right) = \dot{m}_{D_i}^t \,\forall\, i \in \mathscr{N}, t \in \mathscr{T} \tag{8}$$

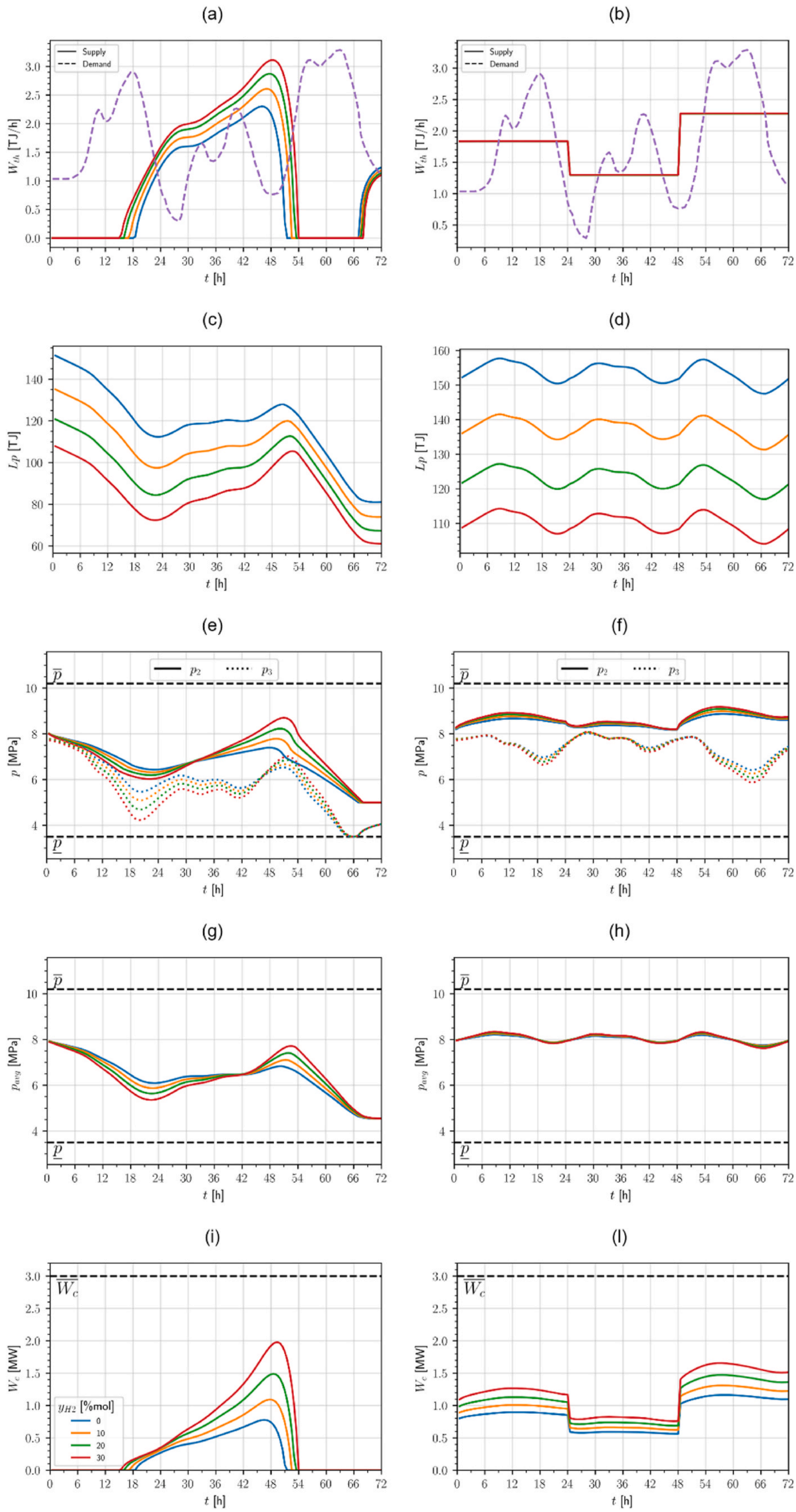

Fig. 6. Case study A results: comparison between OGF that minimizes NG supply (a)-(c)-(e)-(g)-(i) and OGF that minimizes NG supply and maintains the same linepack level at the end of each day (b)-(d)-(f)-(h)-(l). The black dashed lines indicate constraint limits: $\underline{p}$ and $\overline{p}$ represent the minimum and maximum allowable pipeline pressures, respectively, while $\overline{W_c}$ denotes the maximum compressor power. Values are reported in Table 1.

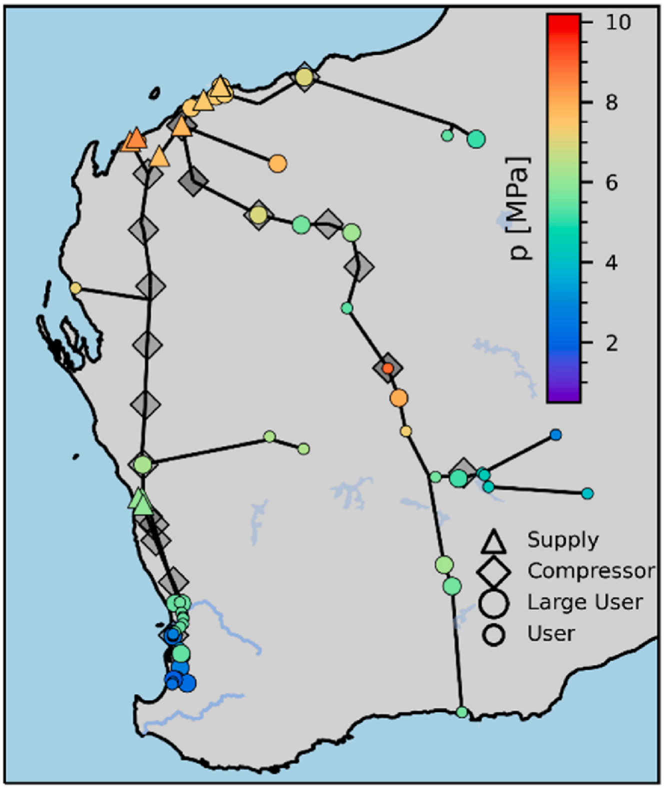

Fig. 7. WA's pressure distribution at peak demand for NG.

Where $\dot{m}_s^t$ represents the mass flow rate supplied to the network by the suppliers associated with node *i*. The summation in the first brackets represents the inflows and outflows associated with pipes connected to node *i*. The summation in the second brackets represents the inflows and outflows associated with compressors connected to node *i*; $\dot{m}_{f_{ij}}^{\ t}$ represents the fuel consumption of the compressors boosting gas from *i* to *j*, while $\dot{m}_{D_i}^{\ t} = \frac{W_{D_i}^{\ t}}{HHV_{mass}}$ represents the nodal mass demand equivalent to a nodal energy demand $W_{D_i}^{\ t}$.

The gas variables stored in the nodes created by the discretization scheme in each pipe are related together by the gas law presented in Equation (9).

$$p_{ij,x}^t = \rho_{ij,x}^t Z_{ij,x}^t R_g T \quad \forall\, ij \in \mathscr{P}, x \in \mathscr{X}, t \in \mathscr{T} \tag{9}$$

Where $Z_{ij,x}^t$ represents the compressibility factor modelled through the well-known Soave-Redlich-Kwong (SRK) equation of state [52] presented in Equation (10). The SRK model was selected for its balance between accuracy and computational efficiency, making it suitable for integration into the nonlinear optimization framework. It provides sufficient accuracy within the operating pressure and temperature ranges considered. Readers interested in higher-fidelity models are referred to GERG-2008 [53], though it comes at a significantly higher computational cost.

$$Z_{ij,x}^3 - Z_{ij,x}^2 + Z_{ij,x} \cdot \left(A_{ij,x}^z - B_{ij,x}^z - {B_{ij,x}^z}^2\right) - A_{ij,x}^z \cdot B_{ij,x}^z = 0 \quad \forall\, ij \in \mathscr{P}, x \in \mathscr{X}, t \in \mathscr{T} \tag{10}$$

Compressors are modelled as connecting elements between two nodes, boosting gas and elevating pressure. Equation (11) represents the relationship between the outlet and inlet pressures of the compressor, with the pressure ratio defined by the variable r_{ij}^t. Equation (12) represents the brake power W_{ij}^t necessary to boost a gas mass flow rate $\dot{m}_{ij}^t$ with a pressure ratio r_{ij}^t considering an adiabatic compression process. Finally, Equation (13) represents the mass flow rate $\dot{m}_{f_{ij}}^{\ t}$ required as fuel in a prime mover of efficiency η_{pm} driving the compressor.

$$P_j^t = r_{ij}^t P_i^t \quad \forall\, ij \in \mathscr{C}, t \in \mathscr{T} \tag{11}$$

$$W_{ij}^t = \frac{\dot{m}_{ij}^t T_i Z_i^t \gamma p_{std}}{\rho_{std} \eta_{c,ij} (\gamma - 1) T_{std}} \cdot \left({r_{ij}^t}^{\frac{\gamma-1}{\gamma}} - 1 \right) \quad \forall\, ij \in \mathscr{C}, t \in \mathscr{T} \tag{12}$$

$$\dot{m}_{f_{ij}}^{\ t} = \frac{W_{ij}^t}{\eta_{pm} LHV_{mass}} \quad \forall\, ij \in \mathscr{C}, t \in \mathscr{T} \tag{13}$$

2.2. Formulation of the OGF problem

Optimizing gas networks from the viewpoint of a neutral operator translates into minimizing the cost of gas supplied to the network (minimizing resource usage) while satisfying demand and ensuring system security.

Considering a time horizon composed of *N* days $\mathscr{G} = \{\mathscr{G}_1, \mathscr{G}_2, .., \mathscr{G}_N\}$, where each $\mathscr{G}_i$ represents the set of timesteps for the i-th day, and the total set of timesteps within this horizon is represented by $\mathscr{T} = \mathscr{G}_1 \cup \mathscr{G}_2 \cup \ldots \cup \mathscr{G}_N$, the OGF model is formulated by introducing the optimization function (14):

$$\min_V \sum_{t \in \mathscr{T}} \left(\left(\sum_{s \in \mathscr{S}} c_s \dot{m}_s^t \right) + c_\omega \omega^t \right) \Delta t \, HHV_{mass} \tag{14}$$

subject to (3)–(13) representing physical constraints, namely the fluid-dynamic model including nodal balance, continuity and momentum equations for pipes, compressors model, and gas properties model; and (15)–(24) representing boundary constraints, namely variables acceptability ranges; and (25)–(26) defining the network operational strategy. In this formulation, variables denoted with an overline (e.g., $\overline{P_i}$) and an underline (e.g., $\underline{P_i}$) represent upper and lower bounds, respectively.

$$\underline{P_i} \le P_i^t \le \overline{P_i} \quad \forall\, i \in \mathscr{N}, t \in \mathscr{T} \tag{15}$$

$$\underline{p_{ij}} \le p_{ij,x}^t \le \overline{p_{ij}} \quad \forall\, ij \in \mathscr{P}, x \in \mathscr{X}, t \in \mathscr{T} \tag{16}$$

$$\underline{\rho_{ij}} \le \rho_{ij,x}^t \le \overline{\rho_{ij}} \quad \forall\, ij \in \mathscr{P}, x \in \mathscr{X}, t \in \mathscr{T} \tag{17}$$

$$\underline{Z} \le Z_{ij,x}^t \le \overline{Z} \quad \forall\, ij \in \mathscr{P}, x \in \mathscr{X}, t \in \mathscr{T} \tag{18}$$

$$0 \le \dot{m}_s^t \le \overline{\dot{m}_s} \quad \forall\, s \in \mathscr{S}, t \in \mathscr{T} \tag{19}$$

$$\underline{\dot{m}_{ij}} \le \dot{m}_{ij,x}^t \le \overline{\dot{m}_{ij}} \quad \forall\, ij \in \mathscr{P}, x \in \mathscr{X}, t \in \mathscr{T} \tag{20}$$

$$\underline{\dot{m}_{ij}} \le \dot{m}_{ij}^t \le \overline{\dot{m}_{ij}} \quad \forall\, ij \in \mathscr{C}, t \in \mathscr{T} \tag{21}$$

$$1 \le r_{ij}^t \le \overline{r_{ij}} \quad \forall\, ij \in \mathscr{C}, t \in \mathscr{T} \tag{22}$$

$$\underline{W_{ij}} \le W_{ij}^t \le \overline{W_{ij}} \quad \forall\, ij \in \mathscr{C}, t \in \mathscr{T} \tag{23}$$

$$\underline{\dot{m}_{f_{ij}}} \le \dot{m}_{f_{ij}}^{\ t} \le \overline{\dot{m}_{f_{ij}}} \quad \forall\, ij \in \mathscr{C}, t \in T \tag{24}$$

$$\omega^t \ge 0 \quad \forall\, t \in \mathscr{T} \tag{25}$$

$$\omega^t \le \left| \sum_{s \in \mathscr{S}} \dot{m}_s^t - \left(\widetilde{\dot{m}}_D^{\mathscr{G}_g} + \sum_{ij \in C} \dot{m}_{f_{ij}}^{\ t} \right) \right| HHV_{mass} \quad \forall\, g \in \mathscr{G}, t \in \mathscr{G}_g \tag{26}$$

Where $V = [\, (\dot{m}_s^t)_{s \in \mathscr{S}};\ (P_i^t)_{i \in \mathscr{N}};\ (p_{ij,x}^t, \rho_{ij,}\ \ x^t, Z_{ij,x}^t, \dot{m}_{ij,x}^t)_{ij\, \in\, \mathscr{P}, x\, \in\, \mathscr{X}};\ (\dot{m}_{ij}^t,\ r_{ij}^t, W_{ij}^t, \dot{m}_{f_{ij}}^{\ t})_{ij \in \mathscr{C}}\,]_{t \in \mathscr{T}}$ represents the variables associated with sup-

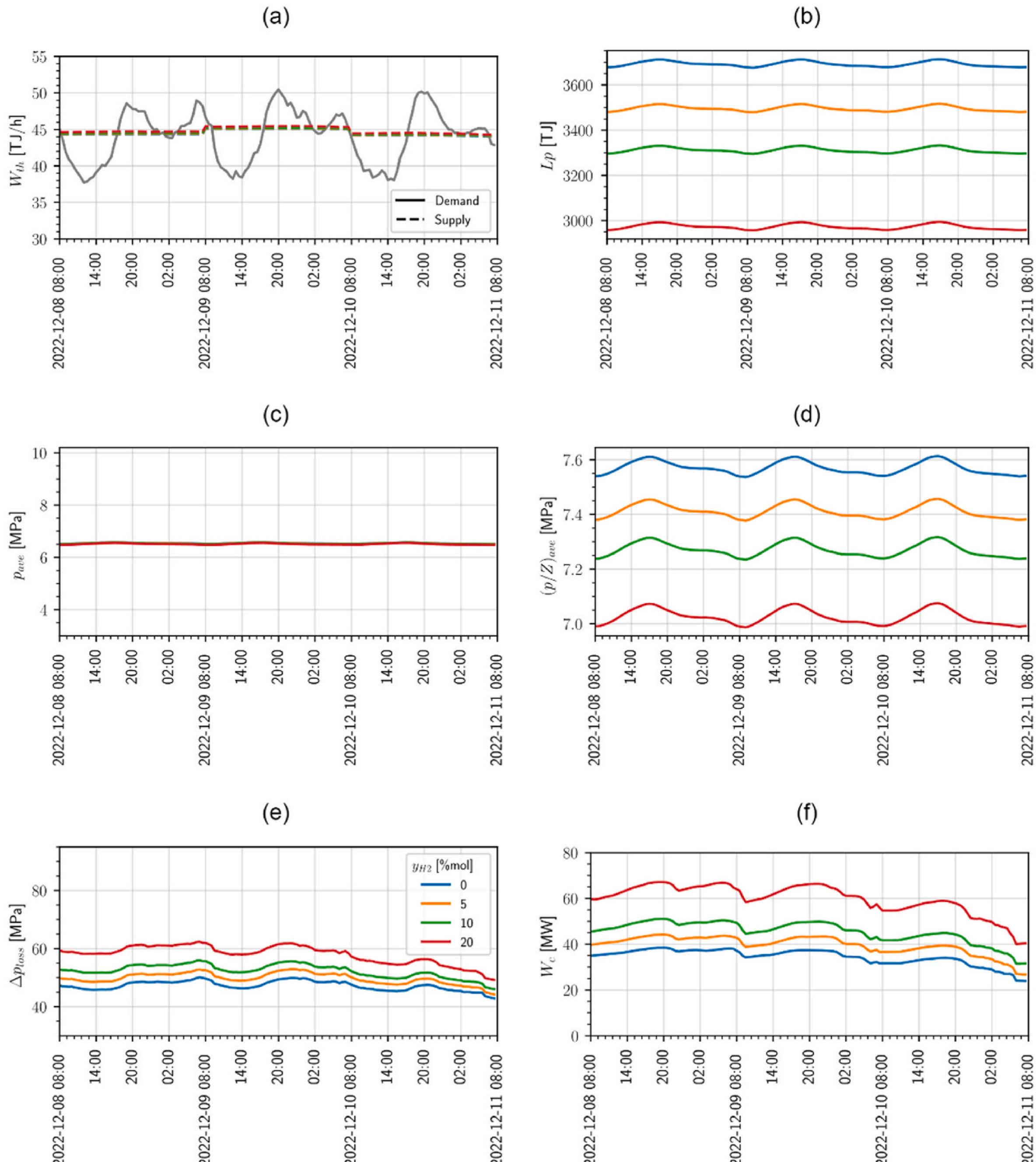

Fig. 8. WA's network results: a) total supply-demand, b) total linepack, c) average pressure in the network, d) average p/Z in the network, e) cumulative pressure losses, f) total compressors power consumption.

ply nodes, real topological nodes, dummy nodes obtained from the pipeline discretization scheme, and compressor variables. Modelling the network from the standpoint of a neutral operator aiming to minimize gas supply may lead to an optimization function that seeks to minimize the gas delivered by utilizing the gas stored in the pipelines (linepack). However, this approach distorts reality and provides unacceptable linepack reductions. To prevent network depressurization and guarantee network flexibility, a term including the support variable ω^t is introduced in the optimization function. The minimization of this term, in light of constraints (25)–(26), translates into the minimization of the difference between the supply and the sum of the average demand $\widetilde{\dot{m}}_D^{\mathscr{G}_g} = \frac{\Delta t}{86400} \sum_{t \in \mathscr{G}_g} \sum_{i \in \mathscr{N}} \dot{m}_{D_i}^t$ and fuel consumption at the compressor stations. Minimizing this difference for each day g guarantees to minimize the difference between the linepack levels at the beginning and end of the day. In other words, while the first term in the optimization function (14) represents the minimization of resources, the second term guarantees to target a constant linepack level at the end of each day in the optimization horizon. The entire modeling and solution pipeline is implemented using Julia v1.8.5 [54] as the programming language. The nonconvex nonlinear programming problem is formulated within JuMP v1.16.0 [55], which serves as the algebraic modeling frontend for defining variables, constraints, and the objective function. The resulting problem is then solved directly using Ipopt v1.5.1, a large-scale nonlinear interior-point solver, with MUMPS as linear solver [56]. Preprocessing tasks such as input data handling, temporal and spatial discretization, and post-processing of the results are managed directly in Julia, outside the JuMP model block. The overall computational

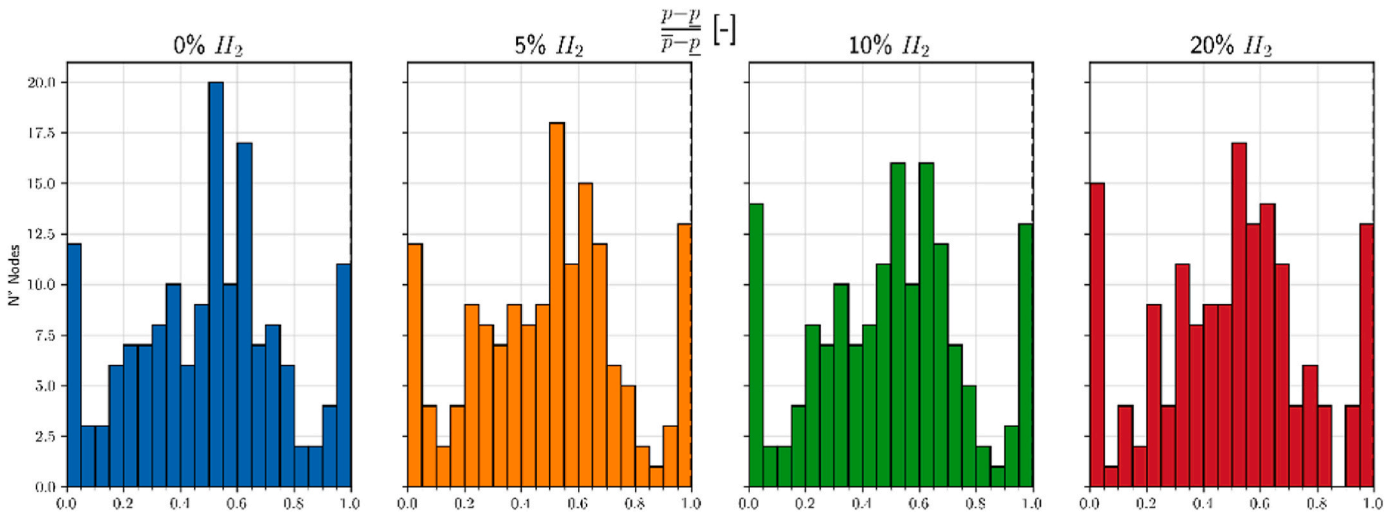

Fig. 9. Distribution of the nodal pressure results at peak demand, normalized based on the nodal pressure constraints.

structure is illustrated in Fig. 2, which outlines the modeling and solution workflow, including the role of Julia, JuMP, and Ipopt in the optimization framework.

3. Case study

This section introduces the two case studies considered in the analysis. The first case study is a simple but representative pipeline system equipped with a compressor station at the supply point. The second case study is the gas transmission network of Western Australia. The NG adopted for both case studies has the following molar composition: CH_4 = 88.396 %, C_2H_6 = 6.554 %, C_3H_8 = 0.00 %, C_4H_{10} = 0.00 %, CO_2 = 1.86 %, N_2= 3.19 %, H_2 = 0.00 %. The volumetric higher heating value and the specific gravity of the gas in standard conditions are HHV = 37.78 MJ/Sm^3 and SG = 0.616, respectively. The model presented in Section 2 is isothermal and the gas temperature assumed in both case studies is T = 15 °C, which is a typical value for buried pipelines. Furthermore, a constant efficiency is adopted for all the compressors (η_c= 0.8) and the prime movers (η_{pm}= 0.3).

3.1. Simple pipeline system

To showcase the model's capabilities and provide a straightforward benchmarking test case, a simple pipeline system inspired by real data is analyzed (Fig. 3). Case study A includes a supply node (Node 1) equipped with a compressor station boosting gas in a pipeline of length L = 450 km, diameter D = 0.35 m and roughness ε = 0.015 mm, to reach the demand node (Node 3). The demand depicted in Fig. 3 exhibits three gas days, showcasing a pseudo-periodic trend with varying average values. A multiday scheduling time horizon was chosen to showcase the supply strategy modelled.

Table 1 outlines the constraints under consideration for case study A. The pressure at the supply node is held constant at 5 MPa. The supply capacity, supposed to be equal to the compressor station and pipeline capacities, is 100 TJ/d. The capacity, expressed as an energy rate capacity, refers to the composition of NG considered in the test case. Therefore, to derive the mass flow rate constraints outlined in the model section expressed in kg/s, readers should refer to the HHV and density at standard conditions of the NG introduced earlier in this section.

3.2. Western Australia gas network

The case study selected to test the robustness and scalability of the model on a large-scale system consists of the WA gas transmission network. Fig. 4 illustrates the network topology: gas is transported from the main supply area in the Dampier zone to various regions via multiple pipelines. The gas travels south-west to Perth via the Dampier to Bunbury Natural Gas Pipeline (DBNGP), north-east to the Telfer mining area via the Telfer Gas Pipeline (TGP), and south-east to the Goldfields mining area via the Goldfields Gas Pipeline (GGP). The network model was developed with the help of industry support, and it consists of 158 nodes, 179 pipelines resulting in a 7560 km network including loops and laterals, 11 NG sources and 21 compressor stations. Details on topology, gas supply capacity and pipelines' capacity can be found in Ref. [57]. Demand was built on data available in Refs. [57,58]. The daily demand given by the Australian Energy Market Operator (AEMO) was assumed to be flat during the day for large industrial and mining users, while a profile inspired by the data available in Ref. [59] was used for the city gate offtakes. Instead, gas-fired generators (GFG) consumption was modelled based on the half-hourly resolution profiles obtained from WA electricity market data [58].

The operation of the system was analyzed over three days. To delete the influence of the steady-state initialization and the finite horizon optimization, following the methodology employed in Refs. [48,60], the three-day optimization horizon was expanded to include one day before and one day after. The five gas days considered begin on December 7, 2022, at 8:00 a.m. and end on December 12, 2022, at 8:00 a.m. Fig. 5 shows the demand profile, highlighting the contributions of industrial users, including mining activities, gate stations, and electricity generation by GFG. The statistical description of the demand is provided in Table 2, demonstrating that the five days chosen are statistically representative of the year 2022.

The model adopts a temporal discretization Δt = 1800 s, i.e., 48-time steps per day with a half-hourly resolution. The gas pipeline maximum discretization length is chosen as Δx = 50000 m. Given the absence of historical data on nodal pressure or linepack, the model validation is based on obtaining mathematically acceptable (feasible) solutions within the set of actual operational constraints.

4. Results

The first analysis presented in this section aims to showcase the features of the model in a simple case study, ensuring replicability. The second case study presents the potentialities of the model to perform analysis on a large-scale real gas network.

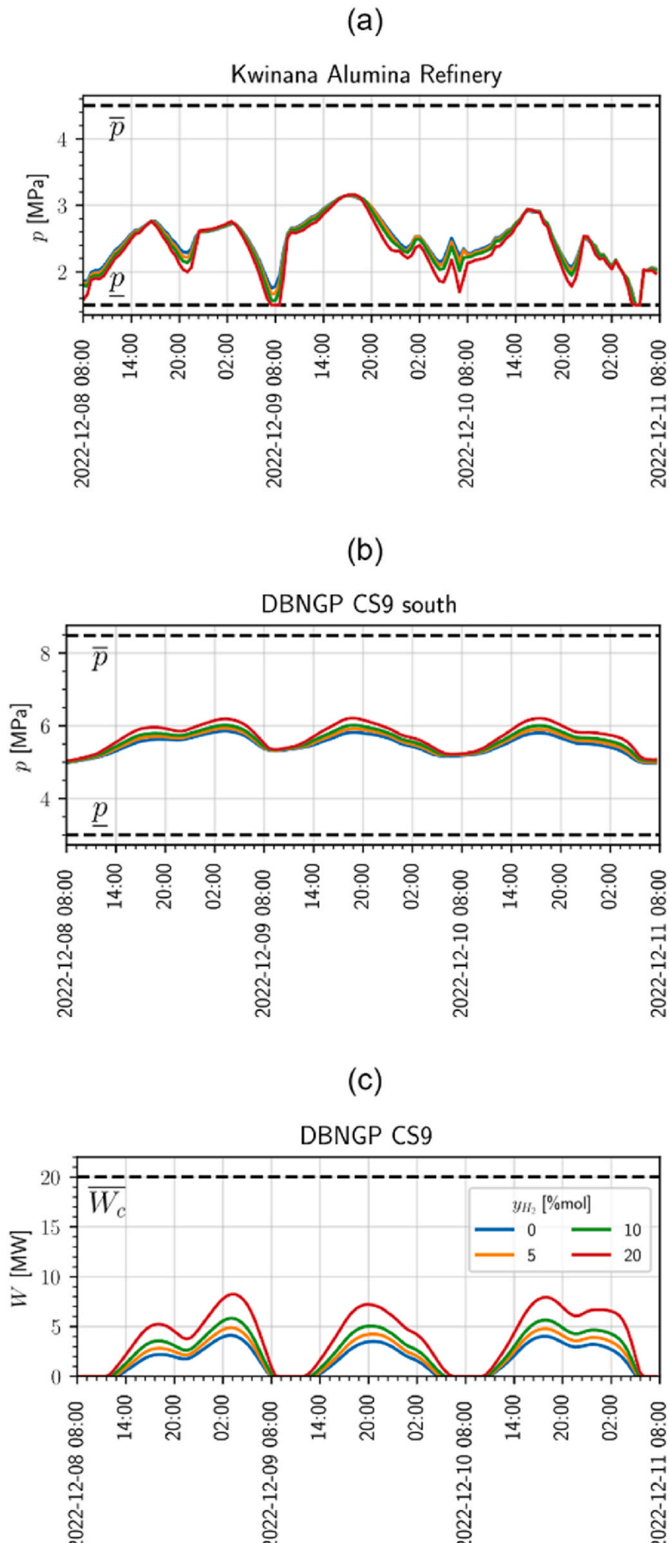

Fig. 10. Nodal pressure at a downstream node (a), upstream node (b) and corresponding compressor power consumption (c). The black dashed lines indicate constraint limits: $\underline{p}$ and $\overline{p}$ represent the minimum and maximum allowable nodal pressures, respectively, while $\overline{W_c}$ denotes the maximum compressor power.

4.1. Case study A: model features

Standard OGF models from the perspective of a neutral operator minimize resource consumption. The model introduced in this paper includes in the optimization function an additional term ω^t that minimizes the difference between the average daily inflows and outflows of the network. To demonstrate the significance of this term, the case study is optimized over a three-day horizon, comparing the results of the model including and not including the ω^t term in the optimization function (14) and constraints (25)–(26).

Fig. 6 shows a comparison of the results of the two models: the first column contains the results of the optimization model that does not include the ω^t term in the optimization function, while the second column contains the results of the optimization model that includes the ω^t term in the optimization function. Fig. 6a shows that without the ω^t term in the optimization function, the gas supply is interrupted for several hours. This phenomenon can be attributed to the model's interpretation of the gas stored in the pipeline (linepack) as a zero-cost gas source. To minimize the gas supplied, the model reduces the linepack (Fig. 6c). However, this strategy results in a reduction of the pipeline pressure, as illustrated in Fig. 6g. As illustrated in Fig. 6e, higher hydrogen concentrations lead to larger volumetric flows and hence steeper pressure drops during the first 20 h. This drives an earlier and more pronounced injection of energy into the pipeline, resulting in higher supply profiles for larger H_2 fractions. In particular, in all H_2 concentration scenarios, the model brings the supply node to cease gas supply until node 3 (offtake node) reaches the minimum pressure constraint, during the final demand peak on the third day (Fig. 6i).

The second column of plots in Fig. 6 shows the significance of incorporating the term ω^t in the optimization function, along with its associated constraints. The supply strategy ensures a relatively flat energy supply, with three levels determined by the different average demand of the three days, as shown in Fig. 6b. This behavior is a direct consequence of the cost function minimization, which includes both the gas supply $\dot{m}_s^t$ and the term ω^t. Constraints (25)–(26) enforce the minimization of the absolute value of the difference between the cumulative energy supplied $\sum_{s\in\mathscr{S}} \dot{m}_s^t \, HHV_{mass}$ and the total energy demand of the network, given by the daily average load $\tilde{\dot{m}}_D^{\mathscr{G}_g} \, HHV_{mass}$ plus the compressor consumption $\sum_{ij\in C} \dot{m}_{f_{ij}}^{t} HHV_{mass}$.

In other words, the model tends to ensure, within the imposed constraints, the same linepack level at the beginning and end of each day (Fig. 6d). Because the energy demand profile is identical across blending scenarios, the optimization yields nearly the same total daily energy supply regardless of the gas mixture. The only differences arise from variations in compressor energy consumption, which slightly increase with hydrogen concentration due to higher flow rates and pressure losses. However, in this case study, such variations are negligible compared to the overall demand and thus do not significantly affect the total supply levels. This is further reflected by the average pipeline pressure, which is proportional to linepack, and remains nearly constant at around 8 MPa (Fig. 6h). A modest oscillation in the average pressure is achieved by increasing the pressure at node 2 using the compressor (Fig. 6l), which compensates for the lower pressure at node 3 resulting from variable pressure losses in the pipeline due to the demand evolution (Fig. 6f).

Fig. 6 also demonstrates the model's capability to capture the different behaviour of NG-H_2 mixtures. As H_2 concentration increases, the linepack decreases due to the lower volumetric HHV and different compressibility factors. Additionally, the compressor's brake power is higher with greater H_2 content caused by the necessity to boost larger flow rates and address higher pressure losses.

4.2. Case study B: the feasibility of H_2 blending in WA

This section outlines the findings of the second analysis, which investigates the feasibility of H_2 blending in the WA gas transmission network and evaluates the robustness and potentialities of the model. Fig. 7 shows a snapshot of the pressure distribution in the network at peak demand transporting NG. The pressure distribution decreases along the DBNGP, TGP, and GGP, reaching the lowest values in the industrial area of Kwinana and the Bunbury area, both located south of Perth.

The model provides feasible solutions for blends containing up to 20 % mol H_2, indicating that the network is fluid-dynamically capable of transporting NG-H_2 blends. Given the NG composition considered, a 20 % mol H_2 blend corresponds to covering 7.80 % of the WA gas network's energy demand. Fig. 8 presents the network results providing insights into system performance. Particularly, Fig. 8a shows the cumulative supply and demand profile of WA's gas network for several NG-H_2 blends. In agreement with the supply strategy imposed by Equations (14)–(25), the energy supply curves are almost flat but slightly different from one another because of the compressors' consumption. As the H_2 content in the mixture increases, so does compressor consumption, resulting in a higher supply curve. The supply strategy ensures the balance between cumulative energy inflows and outflows of the network each gas day, indirectly minimizing the difference between linepack levels at the beginning and end of the day, as depicted in Fig. 8b. As the H_2 molar fraction in the blend increases, the linepack level decreases in alignment with the lower HHV of the gas mixture and the p/Z ratio reduction (Fig. 8d). Nevertheless, it is evident from Fig. 8c that the reduction in linepack does not correspond to a reduction in the average pressure that remains relatively constant at around 6.5 MPa. This outcome can be attributed to the model's effort to adhere to pressure constraints. Notably, Fig. 8e shows that total pressure losses across the network rise by approximately 20 % for the 20 %mol H_2 blend compared to pure NG. To counteract this, compressors increase their output pressure, as permitted by available spare compression capacity, leading to the observed growth in compressor power consumption (Fig. 8f). This increase results from a combination of higher volumetric flow rates and the need for elevated pressure ratios to maintain nodal pressures within acceptable limits.

To validate this interpretation, Fig. 9 presents the nodal pressure distribution across the network during peak demand conditions for various NG-H_2 blending ratios. The pressures are normalized with respect to the allowable operational bounds at each node, such that values approaching 1 correspond to nodes operating near the upper pressure limit, while values close to 0 indicate proximity to the lower pressure threshold. Fig. 9 shows that with higher H_2 concentrations in the mixture, the pressure distribution widens, with more nodes nearing the boundaries set by pressure constraints. In fact, the pressure at the offtake nodes decreases due to increased pressure losses and to mitigate this reduction, compressors boost gas with higher pressure ratios, resulting in higher pressures at the nodes immediately downstream of the compressor stations. Hence, downstream offtake nodes shift towards 0 values in the distribution, while upstream compressor nodes shift towards 1.

To support this interpretation, Fig. 10 illustrates the pressure evolution over time for two nodes in the DBNGP. The node corresponding to an alumina refinery in the Kwinana area serves as an example of a downstream offtake node, while the node situated immediately after CS9 represents the upstream node (Fig. 4). Fig. 10a confirms that, with increasing hydrogen content, the pressure at the offtake node consistently decreases or remains comparable to the pure NG case, reinforcing the observed trend toward the lower bound of the acceptable pressure range shown in Fig. 9. This reduction in offtake pressure is mitigated by increasing the upstream pressure (CS9 outlet pressure), as shown in Fig. 10b. The higher outlet pressure at CS9 translates into higher compressor power consumption (Fig. 10c), suggesting that the overall compressor power consumption of the network shown in Fig. 8f is influenced not only by an increase in volumetric flow rate but also by the higher pressure required downstream of the compressor stations.

5. Conclusions

This paper presents an OGF model suitable for multi-day transient operation scheduling of gas networks. The optimization problem is formulated from the point of view of a neutral operator implementing also a linepack management strategy to maintain flexibility throughout consecutive days. The OGF model's ability to handle homogeneous NG-H_2 mixtures makes it a suitable tool for assessing the fluid-dynamic feasibility of transporting these blends in real networks. Specifically, the developed optimization framework enables gas network operators and policymakers to determine the maximum hydrogen blending limit that does not compromise the flexibility of the gas network by maintaining pressures within design limits. From a modelling perspective, the key insights from this work can be summarized as follows.

- Including a linepack management term in the OGF model's optimization function is crucial to prevent solutions presenting unacceptable progressive linepack reductions. The first case study demonstrates that employing models that overlook linepack constraints may result in unrealistic solutions with low-pressure safety margins. This implies that the optimal solution proposed by standard OGF models may hide a reduced ability of the network to handle unforeseen events such as compressor failures, maintenance, or supply disruptions.
- Assessing the fluid-dynamic feasibility of transporting NG-H_2 blends in large-scale networks can effectively be undertaken by the OGF model presented. The large-scale case study, based on real data from Western Australia's gas transmission network, and solved over a multi-day horizon, demonstrates the model's robustness and capacity to handle real-world problems.

Moreover, the study demonstrates the fluid-dynamic feasibility of transporting blends with up to 20 % mol H_2 in Western Australia's gas network. The implications of this finding are twofold.

- The fluid-dynamic feasibility of transporting a 20 % H_2 blend, potentially covering 7.80 % of WA's gas demand on an energy basis with renewable hydrogen, indicates that the network infrastructure can support partial decarbonization of the gas sector remaining a crucial asset during the energy transition.
- Models able to assess the feasibility of transporting NG-H_2 blends in real networks could open doors to investments in large renewable H_2 projects. In fact, as demonstrated for Western Australia, H_2 can partially offset future NG shortfall arising from the progressive depletion of global NG resources. However, addressing this problem can be of interest to all countries, as NG shortfall scenarios could not only occur due to the progressive depletion of resources but also to emerging geopolitical conflicts.

Future extensions of the model could incorporate the energy equation, multi-source heterogeneous hydrogen injection with compositional tracking, and safety constraints related to material strength. However, these developments would require detailed data on pipeline characteristics and surrounding environmental conditions. In the absence of such data, or if they are inadequately represented, the resulting increase in computational complexity may not necessarily translate into improved accuracy.

CRediT authorship contribution statement

Gabriele Guzzo: Writing – original draft, Visualization, Software, Methodology, Investigation, Formal analysis, Data curation,

Conceptualization. **Sleiman Mhanna:** Writing – review & editing, Software. **Isam Saedi:** Writing – review & editing, Software. **Carlo Carcasci:** Writing – review & editing, Supervision, Resources, Funding acquisition. **Pierluigi Mancarella:** Writing – review & editing, Supervision, Resources, Project administration.

Funding

This research did not receive any specific grant from funding agencies in the public, commercial, or not-for-profit sectors.

Declaration of competing interest

The authors declare that they have no known competing financial interests or personal relationships that could have appeared to influence the work reported in this paper.

References

[1] Pellegrino S, Lanzini A, Leone P. Greening the gas network – the need for modelling the distributed injection of alternative fuels. Renew Sustain Energy Rev 2017;70: 266–86. https://doi.org/10.1016/j.rser.2016.11.243.
[2] Ediger VŞ, Berk I. Future availability of natural gas: can it support sustainable energy transition? Resour Policy 2023;85:103824. https://doi.org/10.1016/j.resourpol.2023.103824.
[3] Gürsan C, De Gooyert V. The systemic impact of a transition fuel: does natural gas help or hinder the energy transition? Renew Sustain Energy Rev 2021;138:110552. https://doi.org/10.1016/j.rser.2020.110552.
[4] Timmerberg S, Kaltschmitt M. Hydrogen from renewables: supply from North Africa to central Europe as blend in existing pipelines – potentials and costs. Appl Energy 2019;237:795–809. https://doi.org/10.1016/j.apenergy.2019.01.030.
[5] Mhanna S, Saedi I, Liu G, Mancarella P. Towards optimal integrated planning of electricity and hydrogen infrastructure for large-scale renewable energy transport. 2022.
[6] Miao B, Giordano L, Chan SH. Long-distance renewable hydrogen transmission via cables and pipelines. Int J Hydrogen Energy 2021;46:18699–718. https://doi.org/10.1016/j.ijhydene.2021.03.067.
[7] Erdener BC, Sergi B, Guerra OJ, Lazaro Chueca A, Pambour K, Brancucci C, et al. A review of technical and regulatory limits for hydrogen blending in natural gas pipelines. Int J Hydrogen Energy 2023;48:5595–617. https://doi.org/10.1016/j.ijhydene.2022.10.254.
[8] Quarton CJ, Samsatli S. Power-to-gas for injection into the gas grid: what can we learn from real-life projects, economic assessments and systems modelling? Renew Sustain Energy Rev 2018;98:302–16. https://doi.org/10.1016/j.rser.2018.09.007.
[9] Gondal IA. Hydrogen integration in power-to-gas networks. Int J Hydrogen Energy 2019;44:1803–15. https://doi.org/10.1016/j.ijhydene.2018.11.164.
[10] Fan X, Cheng YF. Hydrogen pipelines and embrittlement in gaseous environments: an up-to-date review. Appl Energy 2025;387:125636. https://doi.org/10.1016/j.apenergy.2025.125636.
[11] Zhu J, Wang S, Pan J, Lv H, Zhang Y, Han H, et al. Experimental study on leakage temperature field of hydrogen blending into natural gas buried pipeline. Appl Energy 2024;359:122656. https://doi.org/10.1016/j.apenergy.2024.122656.
[12] Topolski K, Reznicek E, Erdener B, San Marchi C, Ronevich J, Fring L, et al. Hydrogen blending into natural gas pipeline infrastructure: review of the state of technology. https://doi.org/10.2172/1893355; 2022.
[13] Cavana M, Mazza A, Chicco G, Leone P. Electrical and gas networks coupling through hydrogen blending under increasing distributed photovoltaic generation. Appl Energy 2021;290:116764. https://doi.org/10.1016/j.apenergy.2021.116764.
[14] Zhang Z, Saedi I, Mhanna S, Wu K, Mancarella P. Modelling of gas network transient flows with multiple hydrogen injections and gas composition tracking. Int J Hydrogen Energy 2022;47:2220–33. https://doi.org/10.1016/j.ijhydene.2021.10.165.
[15] Guandalini G, Colbertaldo P, Campanari S. Dynamic modeling of natural gas quality within transport pipelines in presence of hydrogen injections. Appl Energy 2017;185:1712–23. https://doi.org/10.1016/j.apenergy.2016.03.006.
[16] Mhanna S, Saedi I, Mancarella P, Zhang Z. Coordinated operation of electricity and gas-hydrogen systems with transient gas flow and hydrogen concentration tracking. Elec Power Syst Res 2022;211:108499. https://doi.org/10.1016/j.epsr.2022.108499.
[17] Dancker J, Wolter M. A coupled transient gas flow calculation with a simultaneous calorific-value-gradient improved hydrogen tracking. Appl Energy 2022;316: 118967. https://doi.org/10.1016/j.apenergy.2022.118967.
[18] Saedi I, Mhanna S, Mancarella P. Integrated electricity and gas system modelling with hydrogen injections and gas composition tracking. Appl Energy 2021;303: 117598. https://doi.org/10.1016/j.apenergy.2021.117598.
[19] Wang S, Hui H, Chen T, Zhai J. Multi-period operation of integrated electricity and gas systems with hydrogen blending considering gas composition dynamics. Appl Energy 2025;377:124563. https://doi.org/10.1016/j.apenergy.2024.124563.
[20] Cheli L, Guzzo G, Adolfo D, Carcasci C. Steady-state analysis of a natural gas distribution network with hydrogen injection to absorb excess renewable electricity. Int J Hydrogen Energy 2021;46:25562–77. https://doi.org/10.1016/j.ijhydene.2021.05.100.
[21] Guzzo G, Francesconi M, Carcasci C. Smart management of pressure regulating stations to maximize hydrogen injection in a gas distribution network. Int J Hydrogen Energy 2024;69:626–34. https://doi.org/10.1016/j.ijhydene.2024.04.332.
[22] Clees T, Baldin A, Klaassen B, Nikitina L, Nikitin I, Spelten P. Efficient method for simulation of long-distance gas transport networks with large amounts of hydrogen injection. Energy Convers Manag 2021;234:113984. https://doi.org/10.1016/j.enconman.2021.113984.
[23] Zhou S, Zheng S, Zhang Z, Gu W, Wu Z, Lv H, et al. Consuming the redundant renewable energy by injecting hydrogen into the gas network: a case study of electricity-gas-hydrogen coupled system of Ireland. Int J Hydrogen Energy 2024; 77:1149–62. https://doi.org/10.1016/j.ijhydene.2024.06.078.
[24] Qiu Y, Zhou S, Chen J, Wu Z, Hong Q. Hydrogen-enriched compressed natural gas network simulation for consuming green hydrogen considering the hydrogen diffusion process. Processes 2022;10:1757. https://doi.org/10.3390/pr10091757.
[25] Guzzo G, Cheli L, Carcasci C. Hydrogen blending in the Italian scenario: effects on a real distribution network considering natural gas origin. J Clean Prod 2022;379: 134682. https://doi.org/10.1016/j.jclepro.2022.134682.
[26] Galyas AB, Kis L, Tihanyi L, Szunyog I, Vadaszi M, Koncz A. Effect of hydrogen blending on the energy capacity of natural gas transmission networks. Int J Hydrogen Energy 2023;48:14795–807. https://doi.org/10.1016/j.ijhydene.2022.12.198.
[27] Abd AA, Naji SZ, Thian TC, Othman MR. Evaluation of hydrogen concentration effect on the natural gas properties and flow performance. Int J Hydrogen Energy 2021;46:974–83. https://doi.org/10.1016/j.ijhydene.2020.09.141.
[28] Koo B, Ha Y, Kwon H. Preliminary evaluation of hydrogen blending into high-pressure natural gas pipelines through hydraulic analysis. Energy 2023;268: 126639. https://doi.org/10.1016/j.energy.2023.126639.
[29] Cristello JB, Yang JM, Hugo R, Lee Y, Park SS. Feasibility analysis of blending hydrogen into natural gas networks. Int J Hydrogen Energy 2023;48:17605–29. https://doi.org/10.1016/j.ijhydene.2023.01.156.
[30] Uilhoorn FE. Dynamic behaviour of non-isothermal compressible natural gases mixed with hydrogen in pipelines. Int J Hydrogen Energy 2009;34:6722–9. https://doi.org/10.1016/j.ijhydene.2009.06.062.
[31] Hafsi Z, Elaoud S, Mishra M. A computational modelling of natural gas flow in looped network: effect of upstream hydrogen injection on the structural integrity of gas pipelines. J Nat Gas Sci Eng 2019;64:107–17. https://doi.org/10.1016/j.jngse.2019.01.021.
[32] Elaoud S, Hafsi Z, Hadj-Taieb L. Numerical modelling of hydrogen-natural gas mixtures flows in looped networks. J Petrol Sci Eng 2017;159:532–41. https://doi.org/10.1016/j.petrol.2017.09.063.
[33] Cavana M, Leone P. Solar hydrogen from North Africa to Europe through greenstream: a simulation-based analysis of blending scenarios and production plant sizing. Int J Hydrogen Energy 2021;46:22618–37. https://doi.org/10.1016/j.ijhydene.2021.04.065.
[34] Guzzo G, Saedi I, Mhanna S, Carcasci C, Mancarella P. Hydrogen blending in gas pipelines: fluid-dynamic insights, risks, and recommendations. Int J Hydrogen Energy 2025;120:67–77. https://doi.org/10.1016/j.ijhydene.2025.03.252.
[35] Ríos-Mercado RZ, Borraz-Sánchez C. Optimization problems in natural gas transportation systems: a state-of-the-art review. Appl Energy 2015;147:536–55. https://doi.org/10.1016/j.apenergy.2015.03.017.
[36] Arya AK, Katiyar R, Senthil Kumar P, Kapoor A, Pal DB, Rangasamy G. A multi-objective model for optimizing hydrogen injected-high pressure natural gas pipeline networks. Int J Hydrogen Energy 2023;48:29699–723. https://doi.org/10.1016/j.ijhydene.2023.04.133.
[37] Demissie A, Zhu W, Belachew CT. A multi-objective optimization model for gas pipeline operations. Comput Chem Eng 2017;100:94–103. https://doi.org/10.1016/j.compchemeng.2017.02.017.
[38] Osiadacz AJ, Chaczykowski M. Dynamic control for gas pipeline systems. Arch Min Sci 2016;61:69–82. https://doi.org/10.1515/amsc-2016-0006.
[39] Ehrhardt K, Steinbach MC. Nonlinear optimization in gas networks. In: Bock HG, Phu HX, Kostina E, Rannacher R, editors. Modeling, simulation and optimization of complex processes. Berlin/Heidelberg: Springer-Verlag; 2005. p. 139–48. https://doi.org/10.1007/3-540-27170-8_11.
[40] Wu S, Ríos-Mercado RZ, Boyd EA, Scott LR. Model relaxations for the fuel cost minimization of steady-state gas pipeline networks. Math Comput Model 2000;31: 197–220. https://doi.org/10.1016/S0895-7177(99)00232-0.
[41] Marfatia Z, Li X. On steady state modelling for optimization of natural gas pipeline networks. Chem Eng Sci 2022;255:117636. https://doi.org/10.1016/j.ces.2022.117636.
[42] Tomasgard A, Rømo F, Fodstad M, Midthun K. Optimization models for the natural gas value chain. In: Hasle G, Lie K-A, Quak E, editors. Geometric modelling, numerical simulation, and optimization: applied mathematics at SINTEF. Berlin, Heidelberg: Springer; 2007. p. 521–58. https://doi.org/10.1007/978-3-540-68783-2_16.
[43] Farrokhifar M, Nie Y, Pozo D. Energy systems planning: a survey on models for integrated power and natural gas networks coordination. Appl Energy 2020;262: 114567. https://doi.org/10.1016/j.apenergy.2020.114567.
[44] Correa-Posada CM, Sanchez-Martin P. Integrated power and natural gas model for energy adequacy in short-term operation. IEEE Trans Power Syst 2015;30: 3347–55. https://doi.org/10.1109/TPWRS.2014.2372013.
[45] Liu C, Shahidehpour M, Wang J. Coordinated scheduling of electricity and natural gas infrastructures with a transient model for natural gas flow. Chaos: An

Interdisciplinary Journal of Nonlinear Science 2011;21:025102. https://doi.org/10.1063/1.3600761.
[46] Yang L, Zhao X, Li X, Feng X, Yan W. An MILP-based optimal power and gas flow in electricity-gas coupled networks. Energy Proc 2019;158:6399–404. https://doi.org/10.1016/j.egypro.2019.01.203.
[47] Correa-Posada CM, Sánchez-Martín P. Gas network optimization: a comparison of piecewise linear models.
[48] Ameli H, Qadrdan M, Strbac G. Coordinated operation strategies for natural gas and power systems in presence of gas-related flexibilities. IET Energy Systems Integration 2019;1:3–13. https://doi.org/10.1049/iet-esi.2018.0047.
[49] Mhanna S, Saedi I, Mancarella P. Iterative LP-Based methods for the multiperiod optimal electricity and gas flow problem. IEEE Trans Power Syst 2022;37:153–66. https://doi.org/10.1109/TPWRS.2021.3092760.
[50] Zhang B, Xu N, Zhang H, Qiu R, Wei X, Wang Z, et al. Influence of hydrogen blending on the operation of natural gas pipeline network considering the compressor power optimization. Appl Energy 2024;358:122594. https://doi.org/10.1016/j.apenergy.2023.122594.
[51] Pambour KA, Bolado-Lavin R, Dijkema GPJ. An integrated transient model for simulating the operation of natural gas transport systems. J Nat Gas Sci Eng 2016;28:672–90. https://doi.org/10.1016/j.jngse.2015.11.036.
[52] Soave G. Equilibrium constants from a modified Redkh-Kwong equation of state. Chem Eng Sci 1972.
[53] Kunz O, Wagner W. The GERG-2008 wide-range equation of state for natural gases and other mixtures: an expansion of GERG-2004. J Chem Eng Data 2012;57:3032–91. https://doi.org/10.1021/je300655b.
[54] Bezanson J, Edelman A, Karpinski S, Shah VB. Julia: a fresh approach to numerical computing. SIAM Rev 2017;59:65–98. https://doi.org/10.1137/141000671.
[55] Dunning I, Huchette J, Lubin M. JuMP: a modeling language for mathematical optimization. SIAM Rev 2017;59:295–320. https://doi.org/10.1137/15M1020575.
[56] Wächter A, Biegler LT. On the implementation of an interior-point filter line-search algorithm for large-scale nonlinear programming. Math Program 2006;106:25–57. https://doi.org/10.1007/s10107-004-0559-y.
[57] WA Gas Bulletin Board (WA GBB) n.d. https://aemo.com.au/energy-systems/gas/wa-gas-bulletin-board-wa-gbb (accessed May 25, 2024).
[58] Market data WA n.d. https://aemo.com.au/energy-systems/electricity/wholesale-electricity-market-wem/data-wem/market-data-wa. [Accessed 30 May 2024].
[59] CSIRO. Commonwealth scientific and industrial research organisation, Australian Government n.d. https://www.csiro.au/en/(accessed May 25, 2024).
[60] Cameron I. Using an excel-based model for steady-state and transient simulation.